ELSEVIER

Journal of Power Sources 75 (1998) 44–55

JOURNAL OF POWER SOURCES

Particulate sol–gel synthesis and electrochemical characterization of $LiMO_2$ ($M = Ni, Ni_{0.75}Co_{0.25}$) powders

Chun-Chieh Chang, Prashant N. Kumta *

Department of Materials Science and Engineering, Carnegie Mellon University, Pittsburgh, PA 15213, USA

Received 17 March 1998; accepted 23 April 1998

Abstract

A particulate sol–gel (PSG) process has been developed for synthesizing $LiNiO_2$ and $LiNi_{0.75}Co_{0.25}O_2$ powders. The process is a modified derivative of the colloidal sol–gel technique and yields a precursor that transforms to the oxide by heat treatment at a maximum temperature of 800°C in only 2 h. The synthesized oxides also display good electrochemical activity (135 mA h/g for $LiNiO_2$ and 182 mA h/g for $LiNi_{0.75}Co_{0.25}O_2$) for application in lithium-ion rechargeable batteries. Detailed structural characterization of the as-prepared xerogels have been conducted using Fourier transform infrared spectroscopy (FTIR), while studying their phase evolution behavior during heat treatment using X-ray diffraction (XRD). Results of these studies have been described in this work.

Keywords: Lithium battery; Sol–gel synthesis; Lithium nickel oxide; Lithium nickel cobalt oxide; Electrochemical characterization

1. Introduction

Lithiated transition metal oxides, particularly $LiNiO_2$ and $LiNi_{0.75}Co_{0.25}O_2$ are technically important materials for Li-ion battery applications [1–4]. The former oxide, $LiNiO_2$ has attracted considerable attention over the last few years since it is economically favorable. Moreover, nickel is potentially less toxic and exhibits a higher discharge capacity in comparison to $LiCoO_2$. However, the difficulties encountered in stabilizing the higher oxidation state of Ni during heat treatment makes the control of defect concentration in this material quite a formidable task. These problems have rendered the oxide less favorable for practical applications in rechargeable batteries. On the other hand, in comparison to $LiNiO_2$, $LiNi_{0.75}Co_{0.25}O_2$ is easier to synthesize as reported by us and others [5–7]. There have been several reports in the literature on the synthesis of $LiNiO_2$ using the solid state process employing various precursors and heat treatment conditions, involving different combinations of time, temperature and atmospheres [8]. The vast disparity in the electrochemical properties of the synthesized materials using different precursors reveals the importance of the nature of the precursors on the synthesis of the oxide.

Solid state processes are the preferred traditional methods used for synthesizing these lithiated transition metal oxides. The electrochemical performance of the oxide is largely governed by the chemical stoichiometry, homogeneity, crystallite and particle sizes. Most solid state processes used for synthesizing $LiNiO_2$ generally require prolonged heat treatment time at high temperatures. These high temperature treatments generally do not yield materials exhibiting good electrochemical properties. This is particularly true for $LiNiO_2$ due to its decomposition and loss of lithium thereby leading to cation disorder [9,10]. Furthermore, the high temperature treatments induce growth of crystallites which adversely affect the rate capability due to enhanced polarization losses during cycling. An increase in the crystallite size combined with the cation disorder both contribute to lowering of the kinetics of diffusion. There is therefore a need to identify approaches that can yield the stoichiometric oxide with good control of the crystal chemistry, particle size and morphology. Recently, there has been considerable activity in identifying new low temperature based sol–gel approaches for synthesizing $LiNiO_2$ [11,12].

The particulate sol–gel (PSG) process was developed keeping in mind all the necessary requirements described

* Corresponding author. Tel.: +1-412-268-8739; Fax: +1-412-268-7596; E-mail: kumta@cmu.edu

0378-7753/98/$19.00
PII S0378-7753(98)00091-3

above. It is a modification of the colloidal sol–gel technique for synthesizing $LiNiO_2$ and $LiNi_{0.75}Co_{0.25}O_2$ powders and is based on using organometallic compounds as starting precursors. The technique as described in our earlier work [13,14] consists of dissolving metal carboxylates in water or organic solvents. Hydrolysis can be induced by the addition of lithium hydroxide resulting in the formation of colloidal hydroxide or hydroxy-carboxylate precursors. In the present work, instead of inducing precipitation, clear solutions were obtained which were then subjected to spray drying in order to yield xerogels containing molecularly mixed fine particles. The approach has been successfully used to synthesize $LiNiO_2$ as well as $LiNi_{0.75}Co_{0.25}O_2$ powders. The precursor structure has been analyzed and the phase evolution behavior of the oxide has been studied. The resultant oxide has also been evaluated for its electrochemical performance. Results of these studies have been described in the present manuscript.

2. Experimental

2.1. Materials synthesis

The two oxides, $LiNiO_2$ and $LiNi_{0.75}Co_{0.25}O_2$ studied in this work were prepared using lithium hydroxide monohydrate (Aldrich, 99%) and proper stoichiometric amounts of nickel acetate tetrahydrate (Aldrich, 98%) and cobalt acetate tetrahydrate (Aldrich, 98%) as starting materials. The procedure adapted for synthesizing the materials is shown in Fig. 1. Methanol (400 ml) was used as a solvent to dissolve the stoichiometric amounts of lithium (0.3 mole) and nickel (0.3 mole) or nickel cobalt (a total of 0.3 mole in the case of lithium nickel cobalt oxide) precursors. In the case of $LiNiO_2$, pale green suspensions of colloidal particles were initially obtained when the individually prepared solutions were mixed together. However, upon stirring, the colloidal particles redissolved to obtain a green colored solution. Similarly, the solution prepared for synthesizing $LiNi_{0.75}Co_{0.25}O_2$, was dark purple in color. Since concentrated solutions containing methanol could be potentially flammable and explosive during spray drying, 50 vol % of de-ionized water was added to dilute the methanol solution prior to spray drying. The inlet and outlet temperatures were set at 230°C and 80°C, respectively. A pumping rate of 500 ml/h and a moderate aspiration rate (70 ~ 100 l/min) were employed as the drying conditions in the spray drier (Yamato, mini-spray drier, model ADL31). Heat treatments were conducted in air in the temperature range of 300 to 800°C at increments of 100°C using alumina boats as sample carriers. The dwell time for all of the as-prepared powders was set at 5 h at each of the temperatures in the range of 300–700°C. In the case of $LiNi_{0.75}Co_{0.25}O_2$, the reaction time at 800°C was set at 2 h, while for $LiNiO_2$, the time was varied from 2 to 8 h in order to investigate the variation of the electrochemical properties of the synthesized powders with the heat treatment time.

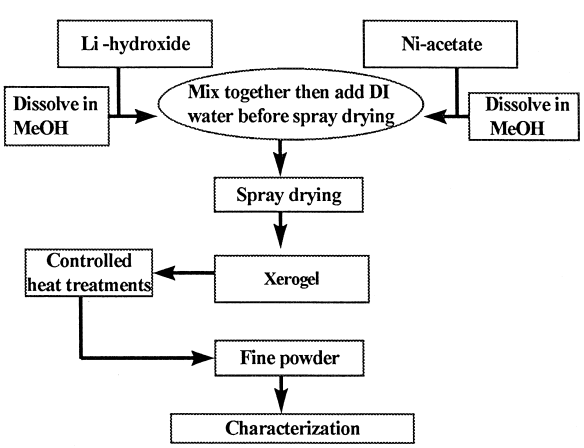

Fig. 1. Schematic of the spray drying process used for synthesizing $LiNiO_2$ and $LiNi_{0.75}Co_{0.25}O_2$.

2.2. Materials characterization

Fourier transform infrared spectroscopy (FTIR, Mattson, Galaxy series FTIR 5000) was conducted using the KBr pressed pellet technique to determine the structure of the as-prepared precursors. Simultaneous thermogravimetric and differential thermal analysis TGA/DTA (TA Instruments, model 2960) was used to monitor the thermal processes occurring during heat treatment. The analysis was conducted in air using ~10 mg of the sample at a heating rate of 5°C/min. The phase evolution as well as structure of the heat treated powders were studied and analyzed using X-ray diffraction (XRD, Rigaku, Japan). The morphology of the resultant powders were observed using a scanning electron microscope (SEM, CamScan, Cambridge, UK), while the specific surface areas were determined implementing the Brunauer, Emmett and Teller (BET) technique (Quantachrome Instruments, NY), respectively.

In order to evaluate the electrochemical characteristics, cathodes were fabricated from the synthesized powders using the formulation comprising 87.1 wt.% synthesized material, 7.6 wt.% acetylene black and 5.3 wt.% copolymer binder (ethylene/propylene copolymer containing 60% ethylene content). The synthesized materials, acetylene black as well as the copolymer were first mixed homogeneously in trichloroethylene (TCE). The solution prepared was coated onto aluminum foils which was then dried. After drying, circular cathodes (usually 0.01 g including the aluminum foil weight of 0.0057 g and 0.003 in. in height with a pellet area of 1 cm^2) were punched out from the cathode-coated aluminum foil. A three electrode Hockey Puck cell design was used [14,15] employing lithium foil as an anode and using 1 M $LiPF_6$ in EC/DMC (with a EC to DMC wt.% ratio of 2 to 1) as the electrolyte. All batteries tested in this study were cycled in the voltage

range from 3.1 to 4.4 V employing a current density of 0.25 mA/cm^2 which were controlled by a potentiostat (Arbin electrochemical instrument). The test batteries were cycled at a C-rate of C/2.

3. Results and discussion

The as-prepared powders employed for synthesizing $LiNiO_2$ and $LiNi_{0.75}Co_{0.25}O_2$, derived by the spray drying process were characterized using TGA, XRD and FTIR. The FTIR data collected on both $LiNiO_2$ and $LiNi_{0.75}Co_{0.25}O_2$ xerogels generated by this process are shown in Fig. 2. Since the results of the analyses of the xerogel powder are very similar for both $LiNiO_2$ and $LiNi_{0.75}Co_{0.25}O_2$, only the results of the as-prepared powders used for synthesizing $LiNiO_2$ are discussed in this section. In Fig. 2, no sharp O–H stretching bands are observed around 3500–3700 cm^{-1} which implies the absence of either lithium hydroxide or nickel hydroxide. By comparing the infrared spectra obtained for both dehydrated nickel acetate and lithium acetate as shown in Fig. 3, one can assign the absorption bands belonging to the acetate groups. The dehydrated acetates were generated by rotary evaporation of the dissolved salts in water using a rotary evaporator (Buchi). According to Nakamoto [16] and Ito and Bernstein [17], bands observed at 3008 and 2931 cm^{-1} can be assigned to ν(CH), and bands seen at 1587 and 1425 cm^{-1} can be assigned to ν_a(COO) and ν_s(COO), respectively. Furthermore, the presence of a strong absorption band below 500 cm^{-1} in the xerogel sample corresponding to the absorption of lithium acetate confirms its existence in the xerogel. Since there is no distinct absorption band characteristic of nickel acetate, its existence from the infrared spectra may not be confirmed. Some other bands observed at 2881 and 2803 cm^{-1} which cannot be assigned to acetate groups could be attributed to the CH_3 vibrations of the methoxy group which will be discussed later.

The TGA/DTA data shown in Fig. 4 reflect a one step weight loss of 41.6% occurring between 230°C and 300°C corresponding to the two broad exothermic reactions. According to the XRD analysis of the xerogel heat treated at 300°C for 5 h as shown in Fig. 5, a mixture of NiO and Li_2CO_3 are observed to be the major products of the decomposition reaction. The results of the IR and thermal analyses of the xerogel however, do not provide sufficient information to conclusively predict its structure and analyze the reactions responsible for the formation of the xerogel. In order to comment on the reaction mechanisms, it was decided to conduct FTIR analysis on an additional sample. This sample was prepared by dissolving lithium hydroxide in methanol and then recovering the powder by evaporating the solvent in a rotary evaporator. The results of the infrared spectra collected on this sample is shown in Fig. 6. It can be seen from Fig. 6 that a mixture of lithium hydroxide and lithium methoxide are formed after dissolving the hydroxide in methanol. The characteristic CH stretching bands at 2790, 2850 and 2920 cm^{-1} [18] confirm the existence of lithium methoxide. Similar analysis conducted on a nickel acetate–methanol solution shows no perceivable reaction as expected. Based on the results of the infrared and TGA analyses described above, it is possible to discuss the reactions that occur leading to the formation of the xerogels. At the same time, it is also possible to analyze the structure of the xerogel. These results can be summarized as follows.

1. The dissolution of lithium hydroxide in methanol leads to the formation of some lithium methoxide, LiOMe (Me = methyl group).

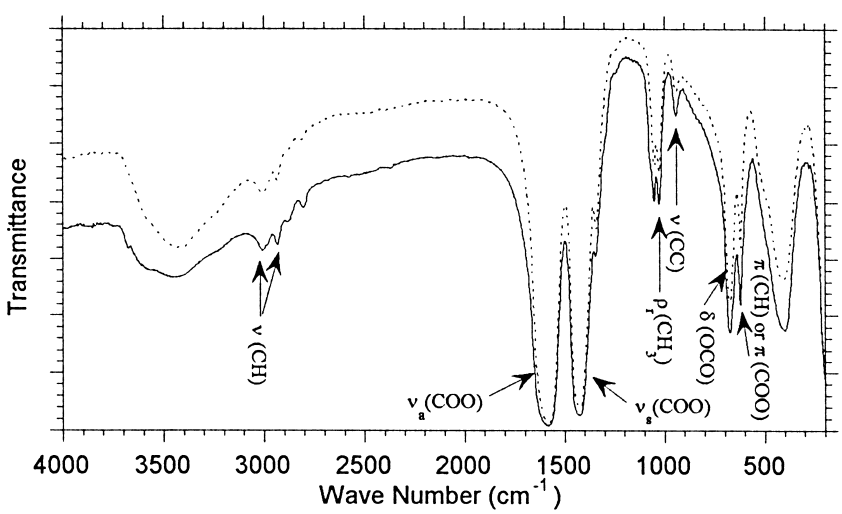

Fig. 2. The FTIR data of $LiNiO_2$ (represented by · · ·) and $LiNi_{0.75}Co_{0.25}O_2$ (represented by ————) xerogels generated by the spray drying process.

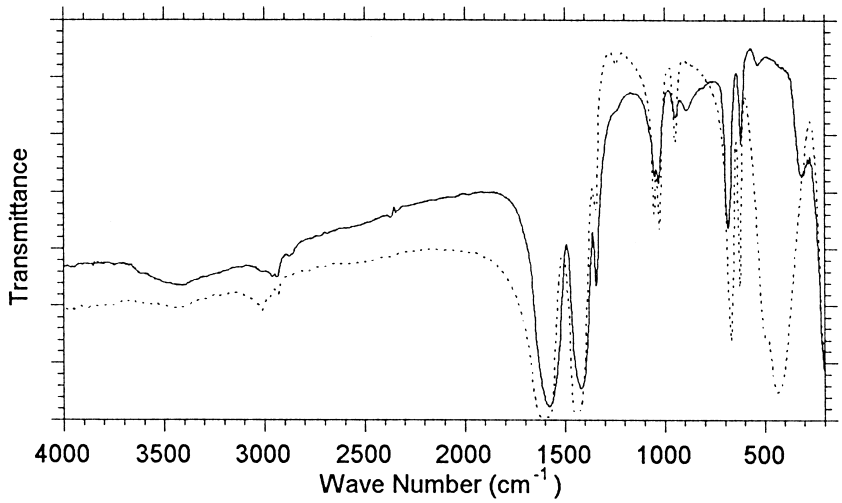

Fig. 3. The IR data of the dehydrated lithium acetate (represented by · · ·) and nickel acetate (represented by ————). By comparing the IR data collected on the xerogel and on the dehydrated lithium acetate and nickel acetate, it is possible to identify the vibrational bands belonging to the acetate groups.

2. Since OH^- and OMe^- are strong nucleophiles, the addition of lithium hydroxide–methanol solution to the nickel acetate–methanol solution can lead to the formation of either Ni(OH)(OAc) or Ni(OMe)(OAc) and Li(OAc), Ac = acetate. The formation of nickel hydroxy acetate has already been identified and reported by us in our previous work [13]. This partially substituted hydroxide is insoluble in water and if it had occurred in the present case, should precipitate out as soon as the lithium hydroxide–methanol solution was transferred to the nickel acetate–methanol solution. In the present work, although precipitation is observed, the precipitates appear to redissolve back into the methanol solution which could imply initially the formation of Ni(OH)(OAc) during the addition of lithium hydroxide–methanol solution to the solution of nickel acetate in methanol. This initially precipitated hydroxy–acetate complex then redissolves back in excess methanol, due to the possible OMe ↔ OH exchange.

3. Since no characteristic OH vibration is observed in the xerogel and the possibility of the loss of acetate groups during drying is low (because of the lack of proton to assist the formation of ester), it can therefore be assumed that the xerogel is largely composed of Ni(OMe)(OAc) and LiOAc in a stoichiometric ratio of lithium:nickel:methoxy groups: acetate groups = 1:1:1:2. Based on the knowledge that the phases present after the

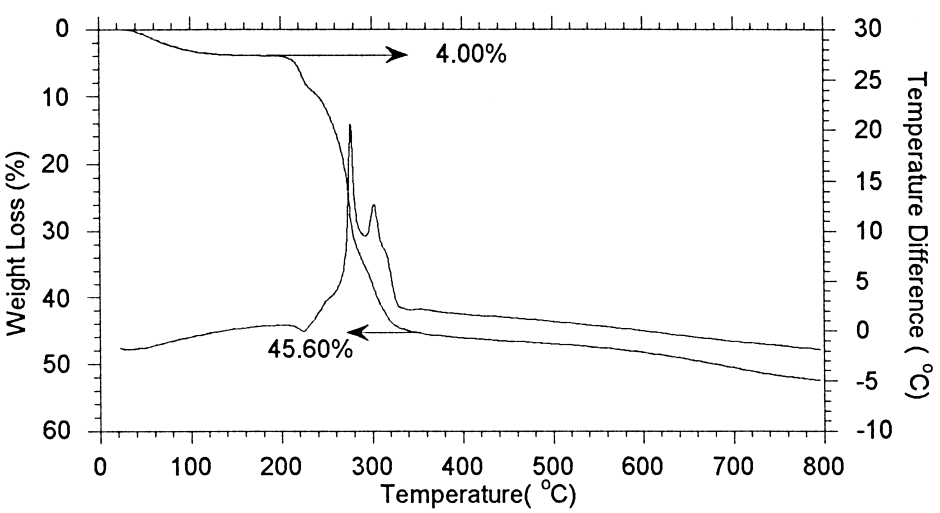

Fig. 4. The TGA/DTA analysis of the $LiNiO_2$ xerogel. A characteristic one step weight loss (41.60%) is observed at ≈ 220°C corresponding to the two broad exotherms.

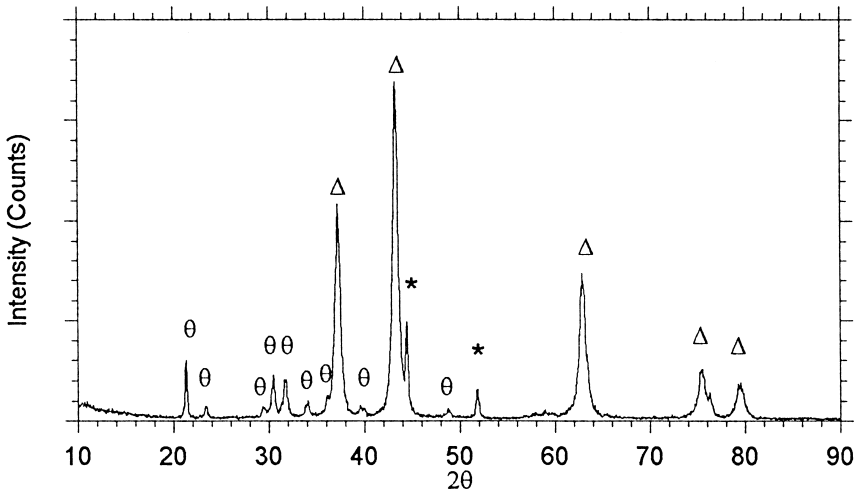

Fig. 5. XRD patterns collected on the $LiNiO_2$ xerogel heat treated at 300°C for 5 h. As shown above, a mixture of NiO and Li_2CO_3 can be seen as the intermediate products obtained after decomposition. (–θ-) represents the Li_2CO_3 phase. (-△-) and (-∗-) represent the NiO phase and the unknown phase, respectively.

decomposition reaction are primarily nickel oxide and lithium carbonate (see Fig. 5), the percent weight loss of the reaction can be expected to be 47.90%, which is however much higher than the weight loss observed from the TGA analysis (41.6%). A possible explanation for this deviation could be the condensation of methoxy groups attached to nickel atoms with the OH groups contributed by lithium hydroxide (source of OH groups) or by the hydrolysis of methoxy groups initiated by the addition of water and the subsequent condensation of hydroxy groups, during the spray drying process at approximately 200°C. The possible formation of Ni–O–Ni linkages due to condensation could lower the molecular weight of the xerogel thereby resulting in a lower percentage of weight loss as observed in the TGA analysis. This assumption is further supported by the absence of OH vibrations observed in the FTIR analysis of the xerogel. This mechanism is very likely since we have also observed the formation of a gel by aging the solution prepared for spray drying. The kinetics of the gelation reaction is very much dependent on the concentration of water. The presence of such condensed species in the xerogel could be confirmed by observing the Ni–O vibrations in the xerogel. It should be mentioned that the Ni–O vibration attributed to the Ni–O–Ni linkages may not be easily identified in the FTIR analysis of the xerogel. This is because of the strong absorption band below 500 cm^{-1}, characteristic of lithium acetate which occurs in the same frequency range as the Ni–O stretching vibration normally observed at 425 and 375 cm^{-1} [19].

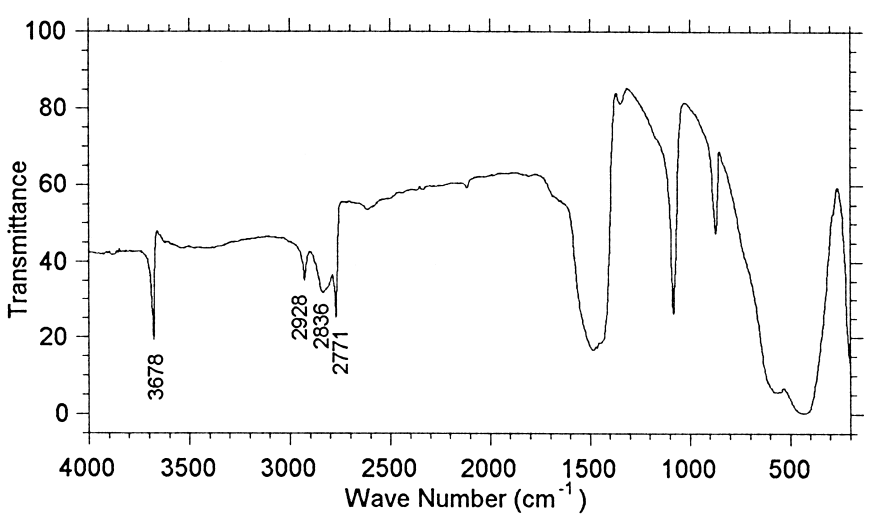

Fig. 6. IR spectra collected on the product obtained after dissolving lithium hydroxide monohydrate in methanol and evaporation of the solvent.

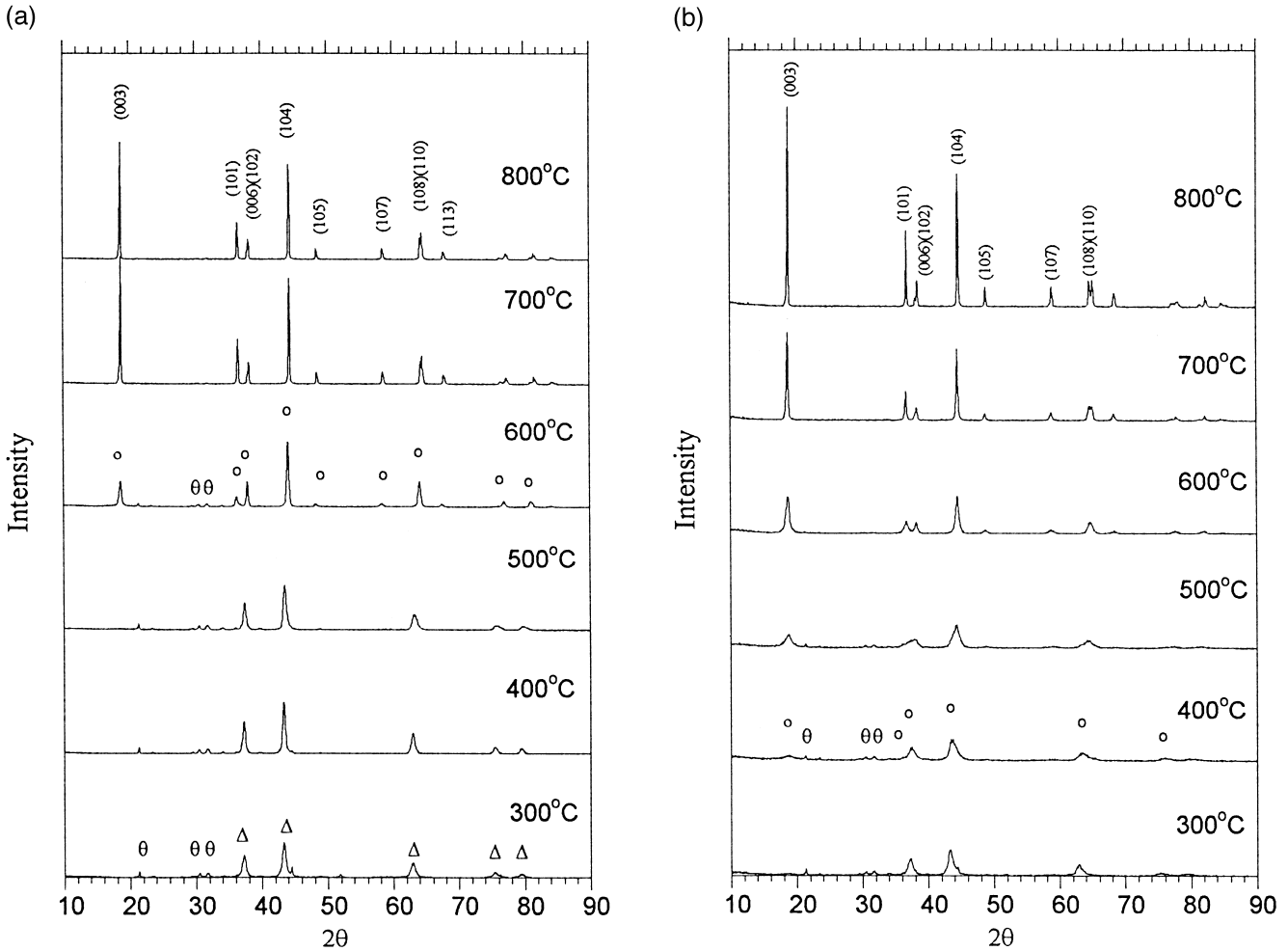

Fig. 7. The phase evolution of (a) $LiNiO_2$ and (b) $LiNi_{0.75}Co_{0.25}O_2$ studied in the temperature range from 300°C to 800°C, respectively. All the heat treatments have been conducted in air for 5 h except for $LiNi_{0.75}Co_{0.25}O_2$ at 800°C which was conducted for only 2 h. (-θ-) represents the Li_2CO_3 phase. (-△-) and (-○-) represent the NiO phase and $LiNiO_2$ phase, respectively.

4. In conclusion, therefore the reactions responsible for the formation of the xerogel during the different stages, can be summarized as follows.

(A) Formation of lithium methoxide. The dissolution of LiOH in methanol leads to formation of some LiOMe:

$$LiOH \cdot H_2O \rightarrow xLiOH + (1-x)LiOMe \quad (1)$$

(B) Precipitation of Ni(OH)(OAc). The mixing of the LiOH–MeOH solution and the $Ni(OAc)_2 \cdot 4H_2O$–MeOH solution leads to precipitation:

$$xLiOH + (1-x)LiOMe + Ni(OAc)_2 \cdot 4H_2O \rightarrow LiOAc + xNi(OH)(OAc)_{ppt} + (1-x)Ni(OMe)(OAc) + 4H_2O \quad (2)$$

(C) Redissolution leading to OH ↔ OMe:

$$Ni(OH)(OAc) + MeOH \rightarrow Ni(OMe)(OAc) + H_2O \quad (3)$$

(D) Dilution with water leading to hydrolysis and condensation during spray drying:

$$nNi(OMe)(OAc) + (n-y)/2H_2O \rightarrow Ni_nO_{(n-y)/2}(OMe)_y(OAc)_n + (n-y)MeOH \quad (4)$$

5. The two exothermic peaks observed in the DTA analysis may represent the decomposition of the nickel species and the lithium acetate formed by virtue of the reactions shown above, which however has not been confirmed in the present study.

The phase evolution behavior of both $LiNiO_2$ and $LiNi_{0.75}Co_{0.25}O_2$ have been studied in the temperature range of 300°C to 800°C and are shown in Fig. 7a and b, respectively. All the heat treatments have been conducted in air at each of the temperatures for a period of 5 h except for the heat treatment at 800°C in the case of $LiNi_{0.75}Co_{0.25}O_2$ which was conducted for only 2 h. Fig. 7b clearly shows the evolution of the rhombohedral $R\bar{3}m$ phase at a lower temperature of 400°C in the case of

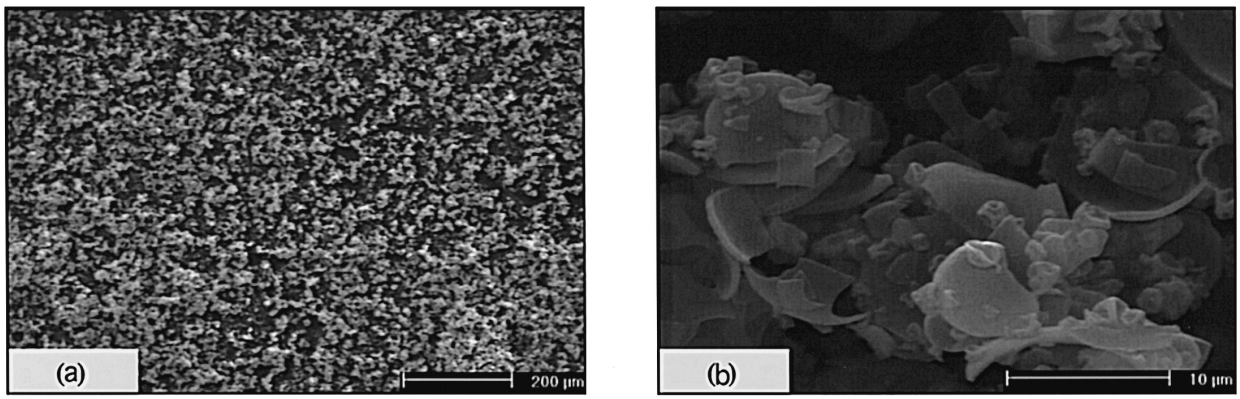

Fig. 8. SEM micrographs of the as-prepared xerogel powders of $LiNiO_2$: (a) morphology of the powders exhibiting a narrow particle size distribution in the range of 7–10 μm. (b) morphology of the precursor particles at a higher magnification of 3 k×.

$LiNi_{0.75}Co_{0.25}O_2$ in comparison to $LiNiO_2$. As shown in Fig. 7a, at 300°C, nickel (or nickel cobalt) oxide and lithium carbonate are the only major phases present in the samples. The broadening of the peaks observed in the XRD analysis for the $LiNi_{0.75}Co_{0.25}O_2$ precursor at 300°C is a clear indication that the nickel cobalt oxide crystallites formed are smaller than the corresponding nickel oxide crystallites. As the temperature is increased to 400°C, the low temperature (LT) phase of $LiNi_{0.75}Co_{0.25}O_2$ begins to evolve, which is in agreement with reports in the literature [20,21]. In comparison to $LiNi_{0.75}Co_{0.25}O_2$, $LiNiO_2$ does not appear to form until the temperature reaches 600°C. However, single phase of both $LiNiO_2$ and $LiNi_{0.75}Co_{0.25}O_2$ is observed at 700°C with lithium carbonate being the only minor secondary phase which may not be clearly identified using X-ray diffraction.

The BET surface area analysis shows that the surface area of the as-prepared powders generated by spray drying

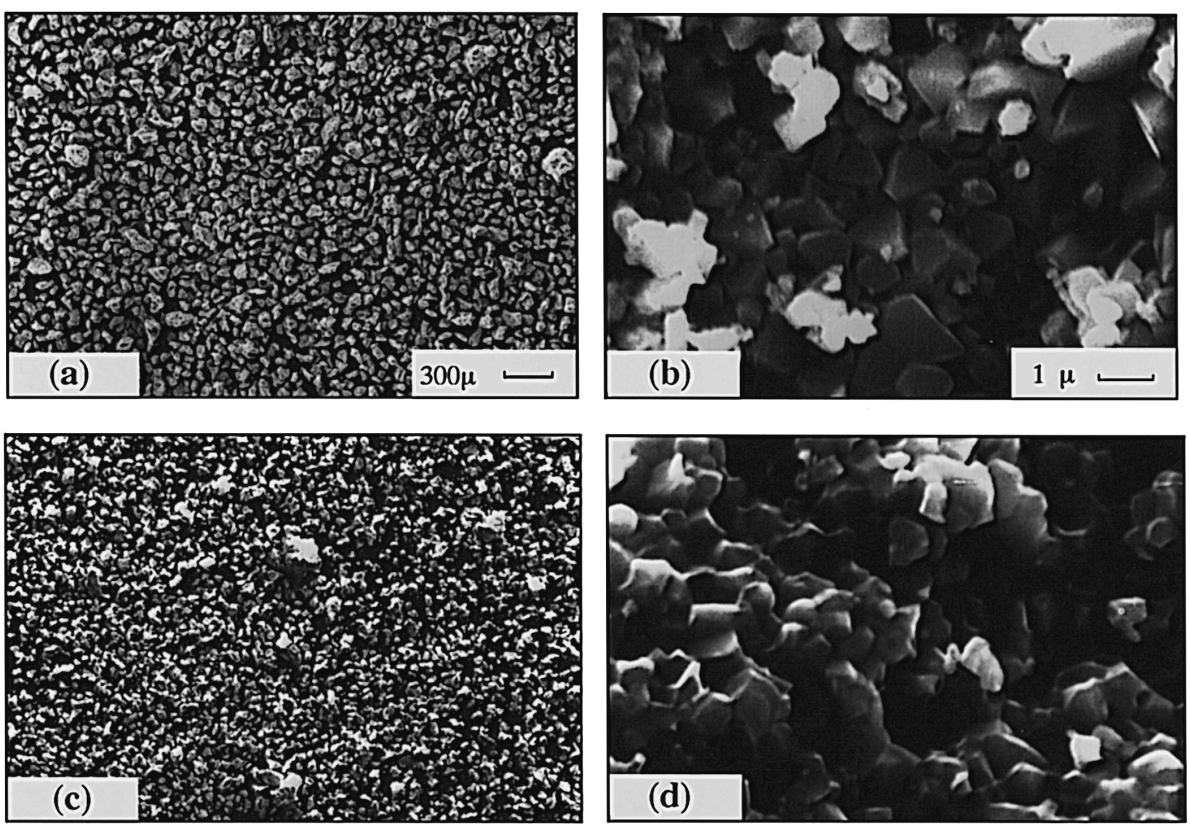

Fig. 9. SEM micrographs of $LiNiO_2$ and $LiNi_{0.75}Co_{0.25}O_2$ powders heat treated in air at 800°C for 2 h; (a) and (c): morphology of $LiNiO_2$ and $LiNi_{0.75}Co_{0.25}O_2$ at a magnification of 30×. From the figure, it can be seen that $LiNiO_2$ (a) powders are generally larger (approximately 50 μm in size) compared to the $LiNi_{0.75}Co_{0.25}O_2$ powders (c). (b) and (d): morphology of $LiNiO_2$ and $LiNi_{0.75}Co_{0.25}O_2$ powders at a magnification of 10 k×, showing faceted crystallites characteristic of both $LiNiO_2$ and $LiNi_{0.75}Co_{0.25}O_2$. The micron markers for (a) and (c), and (b) and (d) are identical.

is approximately 4.74 m^2/g in the case of $LiNiO_2$ and 4.18 m^2/g for $LiNi_{0.75}Co_{0.25}O_2$. After heat treatment at 800°C for 2 h, the surface area of the $LiNiO_2$ powders decreases to 1.31 m^2/g, while that of the $LiNi_{0.75}Co_{0.25}O_2$ powders is lowered to 0.42 m^2/g. The morphology of the as-prepared xerogel powders of $LiNiO_2$ is shown in Fig. 8. Similarly, the morphology of the $LiNiO_2$ and $LiNi_{0.75}Co_{0.25}O_2$ powders obtained after heat treatment at 800°C for 2 h are also shown in Fig. 9 for comparison. From Fig. 8a, it can be seen that the spray dried xerogel particles are very fine and are in the range of 7 μm to 10 μm, signifying the characteristics of the spray drying process. At a magnification of 3 k×, it can be seen that the precursors are essentially composed of hollow spherical particles (10 μm in size). The fractured individual particles are extremely fine and are in the range of 0.5–2 μm.

The morphology of the heat treated powders on the other hand are shown in Fig. 9. At a magnification of 30×, it can be seen that the $LiNiO_2$ particles (~50 μm in size, see Fig. 9a) are generally twice as large as the $LiNi_{0.75}Co_{0.25}O_2$ particles (~25 μm in size, see Fig. 9c). The particle size distribution of the heat treated powders is however narrow in both cases. At a higher magnification of 10 k× as shown in Fig. 9b and d, faceted crystallites can be observed for both $LiNiO_2$ and $LiNi_{0.75}Co_{0.25}O_2$ powders. The crystallite sizes of $LiNi_{0.75}Co_{0.25}O_2$ powders are generally smaller (less than 1 μm, see Fig. 9d) compared to the crystallite size of $LiNiO_2$ powders (approximately 1.5 μm, see Fig. 9b).

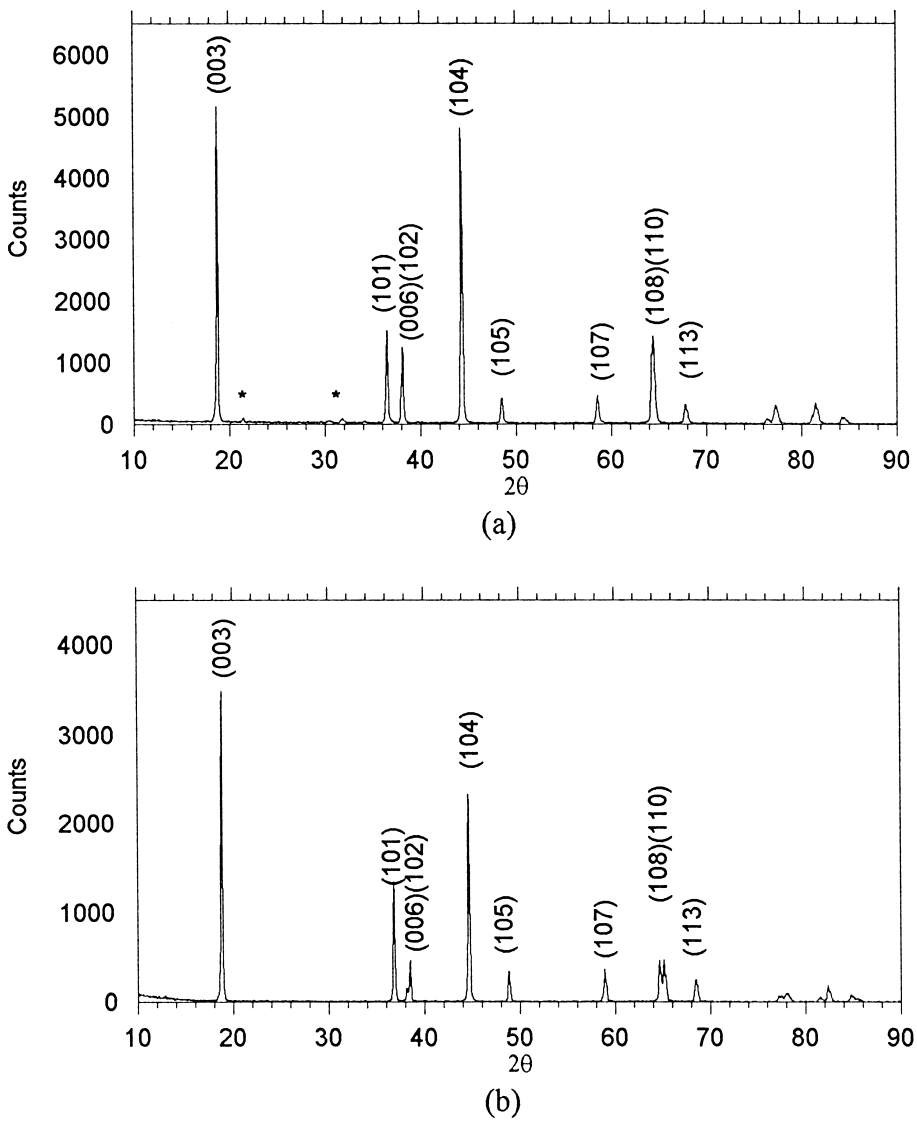

Fig. 10. The XRD patterns of (a) $LiNiO_2$ and (b) $LiNi_{0.75}Co_{0.25}O_2$ powders. Both oxides were obtained after heat treating the xerogels at 800°C for 2 h employing a Li to Ni ratio of 1:1 of the starting materials. Some trace amount of lithium carbonate can still be detected in the XRD pattern of $LiNiO_2$ which is represented by the asterisk sign. The higher integrated intensity of the (104) peak in the $LiNiO_2$ sample implies more disorder of Ni on Li sites (see text for more details).

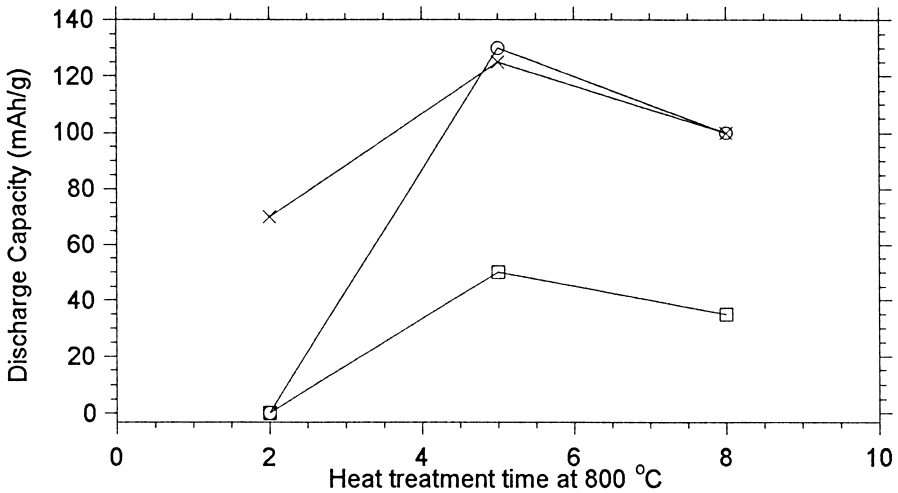

Fig. 11. The variation of heat treatment time and the first discharge capacity using different Li to Ni ratio of the starting materials. (-□-) represents Li:Ni = 1:1. (-○-) represents Li:Ni = 1.05:1. (-×-) represents Li:Ni = 1.08:1, respectively. From the figure it can be seen that the capacity of the material generally increases with the addition of excess Li and with increase in heat treatment time. However, a Li to Ni ratio of 1.08:1 of the starting materials did not improve the property of the material further.

The $LiNiO_2$ and $LiNi_{0.75}Co_{0.25}O_2$ powders obtained after heat treating the spray dried xerogels at 800°C for 2 h were used for electrochemical characterization. These xerogels were synthesized using stoichiometric amounts of lithium, nickel and cobalt precursors. The $LiNi_{0.75}Co_{0.25}O_2$ powders show a first discharge capacity of 182 mA h/g whereas $LiNiO_2$ powders do not exhibit any electrochemical capacity. The XRD data for both $LiNiO_2$ and $LiNi_{0.75}Co_{0.25}O_2$ powders are shown in Fig. 10. The integrated peak intensity ratio of $(003)/(104) = 0.895$ for the $LiNiO_2$ sample, which corresponds to a lithium content of 0.891 using the formula reported by Dahn et al. [22], suggesting the severity of the disorder of Ni on Li sites. Since the misposition of Ni on Li sites may be caused by deficiency of Li which is reported to be volatile at elevated temperatures, a series of experiments were conducted based on modifying the heat treatment time and varying the Li to Ni ratio in the starting material. Three different ratios were attempted, namely Li:Ni = 1:1, 1.05:1 and 1.08:1. Similarly, the heat treatment time at 800°C for each case was set at 2 h, 5 h and 8 h, respectively. The effect of heat treatment time on the first discharge capacity using different Li to Ni ratios of the starting materials is shown in Fig. 11. From the figure it is seen that the capacity of the material generally increases by the incorporation of excess Li. However, a Li:Ni ratio of 1.08:1 in the starting materials did not seem to improve the capacity of the oxide any further.

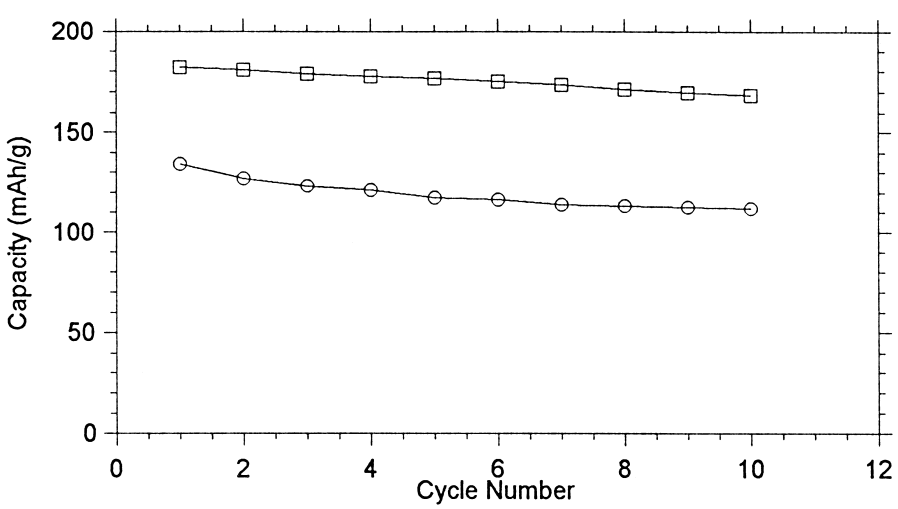

Fig. 12. The capacity vs. cycle number plot for the first 10 cycles of the best $LiNiO_2$ and $LiNi_{0.75}Co_{0.25}O_2$ synthesized in this study. A capacity fade of 1.71%/cycle was observed for $LiNiO_2$ and only 0.84%/cycle was observed for $LiNi_{0.75}Co_{0.25}O_2$. (-○-). represents the profile for $LiNiO_2$ and (-□-) represents the plot for $LiNi_{0.75}Co_{0.25}O_2$.

The best first discharge capacity for $LiNiO_2$ obtained in this study is ≈135 mA h/g. The oxide was synthesized using a ratio of Li:Ni = 1.05:1 and was obtained after heat treatment at 800°C for 5 h. The capacity vs. cycle number plot for the first 10 cycles of the best $LiNiO_2$ and $LiNi_{0.75}Co_{0.25}O_2$ material synthesized in this study is shown in Fig. 12. The $LiNi_{0.75}Co_{0.25}O_2$ used for electrochemical characterization was heat treated at 800°C for 2 h. In comparison to $LiNiO_2$, $LiNi_{0.75}Co_{0.25}O_2$ exhibits a better cycling behavior. The mixed oxide shows a first discharge capacity of 182 mA h/g which fades to only 168 mA h/g in 10 cycles thus indicating a fade of 0.84%/cycle. On the other hand, $LiNiO_2$ shows a first discharge capacity of 134 mA h/g which fades to 112 mA h/g after 10 cycles indicating a fade of 1.71%/cycle. Fig. 13 shows a plot of the voltage vs. Li content for the first two cycles for both $LiNiO_2$ and $LiNi_{0.75}Co_{0.25}O_2$. The average voltage of the second cycle (charge and discharge) was calculated using the formula:

$$\bar{V} = \left(\int_{Q_1}^{Q_2} V \mathrm{d}Q \right) \Big/ Q$$

where $\bar{V}$ is the average voltage and Q is the charge in Coulombs. Using this formula, the average voltage for $LiNiO_2$ during charge and discharge was determined to be 3.94 V and 3.78 V, respectively, in comparison to 3.89 V and 3.78 V for $LiNi_{0.75}Co_{0.25}O_2$.

Based on the calculation of the average voltage, it can be seen that polarization losses are more severe in the case of $LiNiO_2$ in comparison to $LiNi_{0.75}Co_{0.25}O_2$. This could be attributed to the combined problem of disorder of Ni on Li sites and the existence of residual lithium carbonate which tends to cover some of the $LiNiO_2$ particles as

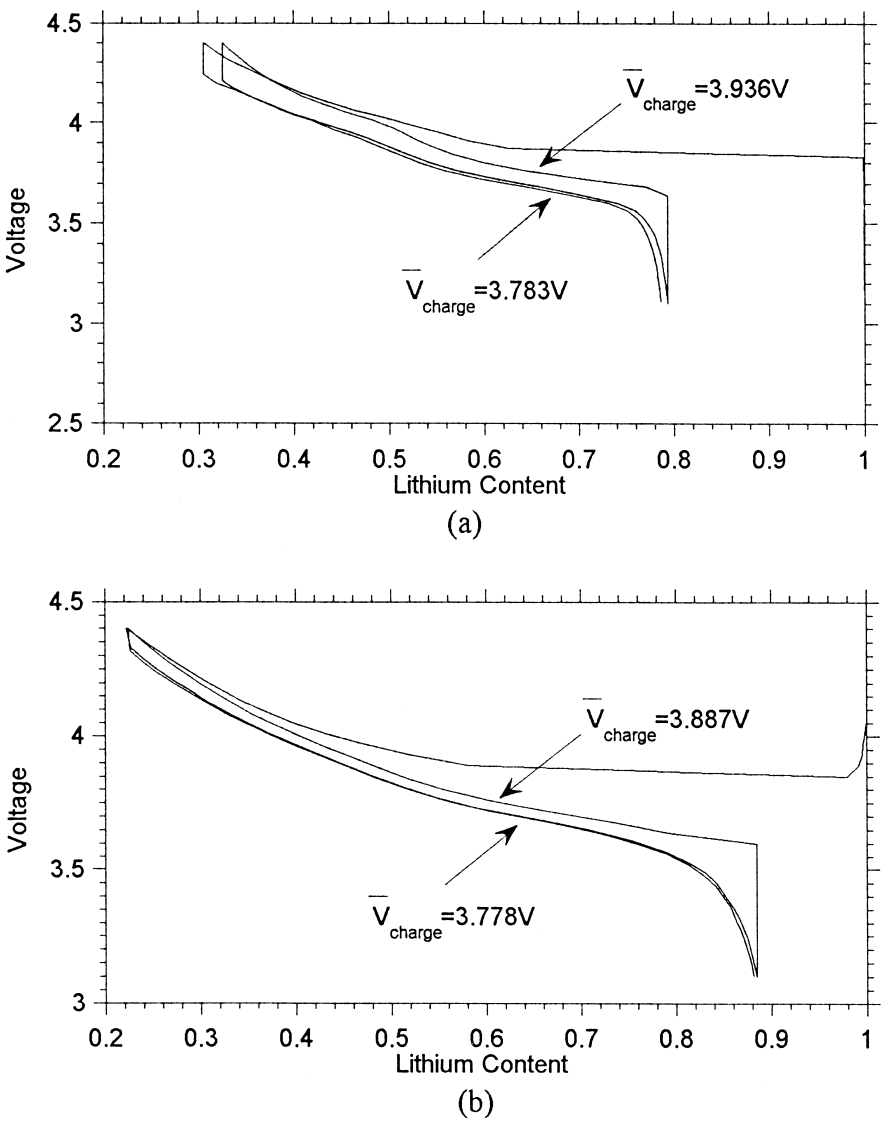

Fig. 13. Plot of the voltage vs. Li content for the first two cycles for both (a) $LiNiO_2$ and (b) $LiNi_{0.75}Co_{0.25}O_2$.

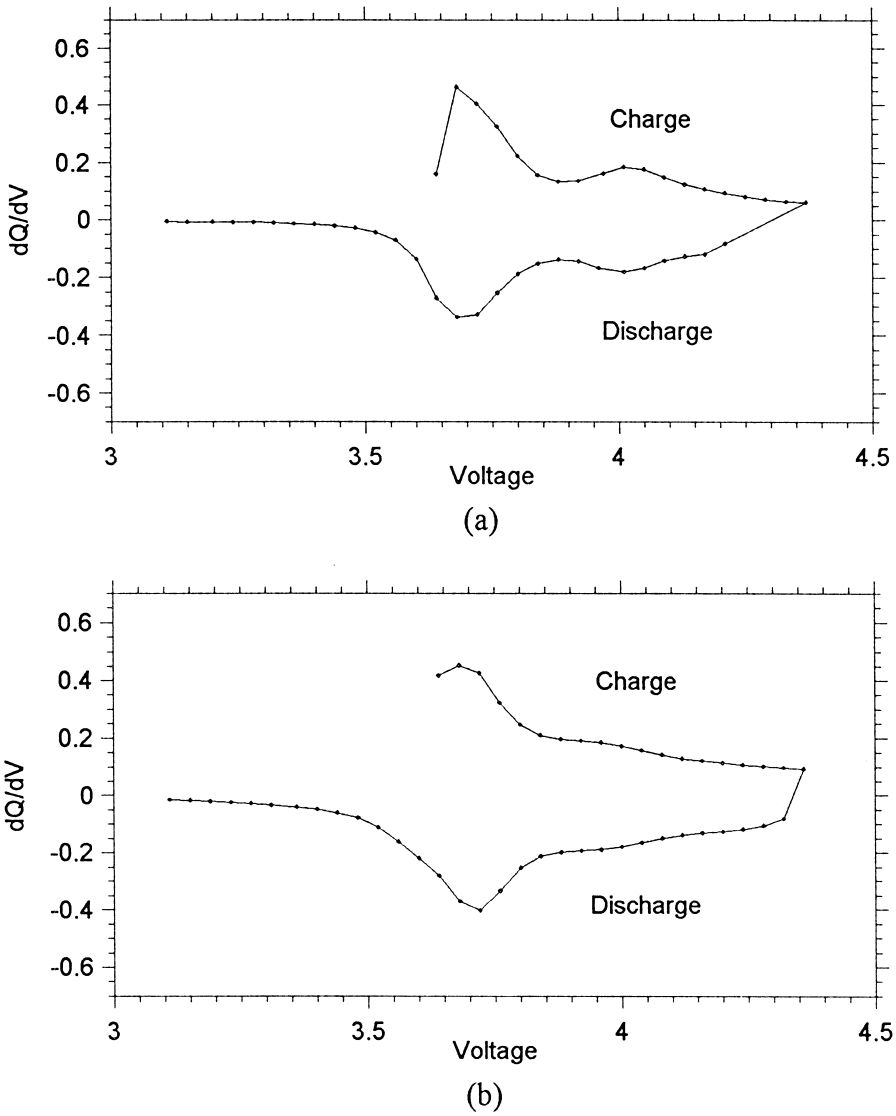

Fig. 14. The dQ/dV vs. V plot for both (a) $LiNiO_2$ and (b) $LiNi_{0.75}Co_{0.25}O_2$ cathodes. A single peak is observed in the case of $LiNi_{0.75}Co_{0.25}O_2$ implying the absence of any phase transformation during cycling. In the case of $LiNiO_2$, two peaks are observed compared to several peaks reported in the literature which could be attributed to the effect of delay of phase transformation caused by the disorder of Ni on Li sites. See text for details.

reported by us in our previous work [13]. The dQ/dV vs. V plots for both $LiNiO_2$ and $LiNi_{0.75}Co_{0.25}O_2$ samples are shown in Fig. 14a and b, respectively. A single peak is observed in the case of $LiNi_{0.75}Co_{0.25}O_2$ which implies the absence of any phase transformation occurring during cycling. On the other hand, in the case of $LiNiO_2$, two peaks are observed in comparison to several peaks reported in the literature [23]. This could be attributed to the effect of delay of phase transformation caused by the disorder of Ni on Li sites as reported by Hirano et al. [24].

In addition, in the synthesis of $LiNiO_2$, the stability of the Li_2CO_3–NiO interface prevents the attainment of the $R\bar{3}m$ structure easily. As a result, the material exhibits poor activity. However, the addition of excess lithium helps to alleviate the problem to some extent. Work is currently in progress to identify heat treatment protocols to accelerate the kinetics of the reaction between the intermediate products leading to the formation of $LiNiO_2$ at lower temperatures.

4. Conclusions

The particulate sol–gel (PSG) based spray drying process has been successfully utilized for synthesizing $LiNiO_2$ and $LiNi_{0.75}Co_{0.25}O_2$. Based on the structural characterization of the xerogel powders generated immediately after spray drying using FTIR, TGA/DTA and XRD, the possibility of the formation of Ni–O–Ni linkages in the xerogel can be expected. Nickel (in the case of $LiNiO_2$) oxide and lithium carbonate are the only major phases present in the material after the decomposition reaction that occurs at

230°C. The formation of $LiNi_{0.75}Co_{0.25}O_2$ at the low temperature of 400°C in comparison to $LiNiO_2$ which forms at 600°C implies the readily oxidizable character of Ni^{2+} and Co^{2+} in $LiNi_{0.75}Co_{0.25}O_2$. The morphology of the synthesized $LiNiO_2$ and $LiNi_{0.75}Co_{0.25}O_2$ powders comprise faceted crystallites characteristic of the $R\bar{3}m$ structure. An initial capacity of 135 mA h/g and 182 mA h/g for $LiNiO_2$ and $LiNi_{0.75}Co_{0.25}O_2$, respectively demonstrate the potential viability of the PSG process for synthesizing lithiated transition metal oxide powders for Li-ion rechargeable battery application.

Acknowledgements

The authors gratefully acknowledge the support of ARPA (Contract # N00014-94-1-0773), and NSF (Grants CTS-9309073, CTS-9700343, and DMR-9301014) and Changs Acending, Taiwan, for this research. Technical assistance of Eveready Battery is also acknowledged.

References

[1] M. Broussely, F. Perton, P. Biensan, J.M. Bodet, J. Labat, A. Lecerf, C. Delmas, A. Rougier, J.P. Peres, J. Power Sources 54 (1995) 109–114.
[2] T. Ohzuku, A. Ueda, M. Nagayama, Y. Iwakoshi, H. Komori, Electrochimica Acta 38 (1993) 1159–1167.
[3] B. Banov, J. Bourilkov, M. Mladenov, J. Power Sources 54 (1995) 268–270.
[4] D. Caurant, N. Baffier, B. Garcia, J.P. Pereira-Ramos, Solid State Ionics 91 (1996) 45–54.
[5] Chun-Chieh Chang, N. Scarr, P.N. Kumta, Proc. Symp. Batteries for Portable Applications and Electric Vehicles, 1997, Vol. 97–98, p. 163, The Electrochemical Society, Pennington, NJ, USA.
[6] C. Delmas, I. Saadoune, Solid State Ionics 53–56 (1992) 370–375.
[7] R. Koksbang, J. Barker, H. Shi, M.Y. Saidi, Solid State Ionics 84 (1996) 1–21.
[8] T. Ohzuku, A. Ueda, M. Nagayama, J. Electrochem. Soc. 140 (1993) 1862–1870.
[9] S. Yamada, M. Fujiwara, M. Kanda, J. Power Sources 54 (1995) 209–213.
[10] W. Li, J.N. Reimer, J.R. Dahn, Phys. Rev. B 46 (1992) 3236–3246.
[11] T. Ohzuju, A. Ueda, M. Nagayama, Y. Iwakoshi, K. Sawai, Chem. Exp. 7 (1992) 689–692.
[12] X. Xiao, Y. Xu, J. Mater. Sci. 31 (1996) 6449–6454.
[13] Chun-Chieh Chang, N. Scarr, P.N. Kumta, Solid State Ionics (1998) in press.
[14] D. Gallet, A. Waghray, P.N. Kumta, G.E. Blomgren, M. Setter, J. Power Sources, (1998) in press.
[15] D. Gallet, A. Waghray, P.N. Kumta, G.E. Blomgren, M. Setter, Proc. Symp. The Role of Ceramics in Electrochemical Devices, 1996, Vol. 65, p. 177, American Ceramic Society, Cincinnati, OH, USA.
[16] K. Nakamoto, Infrared and Raman Spectra of Inorganic and Coordination Compounds, Wiley, New York, USA, 1986.
[17] K. Ito, H.J. Bernstein, Can. J. Chem. 34 (1956) 170–178.
[18] D. Aurbach, M.L. Daroux, P.W. Faguy, E. Yeager, J. Electrochem. Soc. 134 (1987) 1611–1620.
[19] R.W. Adams, R.L. Martin, G. Winter, Australian J. Chem. 20 (1967) 773–774.
[20] R.J. Gummow, M.M. Thackeray, Solid State Ionics 53–56 (1992) 681–687.
[21] R.J. Gummow, M.M. Thackeray, J. Electrochem. Soc. 140 (1993) 3365–3368.
[22] J.R. Dahn, U. von Sacken, C.A. Michal, Solid State Ionics 44 (1990) 87–97.
[23] W. Ebner, D. Fouchard, L. Xie, Solid State Ionics 69 (1994) 238–256.
[24] A. Hirano, R. Kanno, Y. Kawamoto, Y. Takeda, K. Yamaura, M. Takano, K. Ohyama, M. Ohashi, Y. Yamaguchi, Solid State Ionics 78 (1995) 123–131.